

# Attention-space Contrastive Guidance for Efficient Hallucination Mitigation in LVLMs

Yujin Jo, Sangyoob Bae, Taesup Kim\*

Graduate School of Data Science, Seoul National University

## Abstract

*Hallucinations in large vision–language models (LVLMs) often arise when language priors dominate over visual evidence, causing object misidentification and visually inconsistent descriptions. We address this issue by framing hallucination mitigation as contrastive guidance, steering generation toward visually grounded and semantically faithful text. This approach regulates the model’s internal behavior by reducing over-dependence on language priors and contrasting visually grounded with language-only representations. We propose Attention-space Contrastive Guidance (ACG), a single-pass mechanism that operates within self-attention layers to construct both vision–language and language-only attention paths in a single forward computation. This integration enables computationally efficient guidance directly embedded in the model’s representation contextualization. To correct approximation bias introduced by the single-pass formulation, we further apply an orthogonalized correction that removes components aligned with the language-only path, selectively amplifying visual contributions. Experiments on the CHAIR and POPE benchmarks show that ACG achieves state-of-the-art faithfulness and caption quality while significantly reducing computational cost. Our method establishes a principled and efficient alternative, reducing latency by up to 2x compared to prior contrastive decoding methods that require multiple forward passes.*

## 1. Introduction

Large vision–language models (LVLMs) have recently demonstrated impressive performance across a wide range of multimodal tasks, from open-ended visual question answering and captioning to instruction following and tool use [1, 2, 6, 15, 19, 37]. By combining strong visual encoders with powerful large language models, these systems can describe complex scenes, follow multimodal instructions, and reason over images using natural language. De-

spite this rapid progress, LVLMs still suffer from a critical failure mode: hallucination, where the model generates text that is inconsistent with the visual evidence, such as confidently describing objects that are not present in the image [12, 17, 24, 28]. Such failures substantially undermine the reliability and trustworthiness of LVLMs and are especially problematic in safety-critical applications such as medical imaging, autonomous driving, and robotics, where image-grounded reasoning is essential [39].

At a high level, hallucinations often occur when the model over-relies on language priors acquired during large-scale text pre-training and under-utilizes the actual visual evidence [3]. The model fills in plausible but unobserved objects based on co-occurrence statistics rather than strictly conditioning on the input image. In this sense, hallucinations can be viewed as a failure of controlled generation: the model’s outputs are not sufficiently constrained by the given visual condition, and its generative behavior drifts toward language-only biases. A straightforward way to reduce hallucinations is to modify the model itself, for example via architectural changes or additional fine-tuning on hallucination-focused datasets. Recent works follow this direction by aligning LVLMs with human or synthetic preferences through RLHF optimization or contrastive learning [8, 28, 33]. While such approaches can be effective, they are costly and inflexible: they require access to model parameters and expensive retraining on carefully constructed preference data.

This has motivated a growing line of training-free, inference-time methods that aim to steer a fixed LVLM without modifying its parameters. More closely related to our work are logit-level guidance and contrastive decoding methods [14, 21, 22, 31]. These approaches compare logits under image-conditioned and text-only inputs to penalize language-biased continuations and promote outputs that are better aligned with the conditioning signal. Logit-level methods, however, suffer from two key limitations. First, they operate only at the final output layer, after biases have accumulated across all layers. As a result, they provide a global, post-hoc correction that cannot directly address

\*Corresponding author.

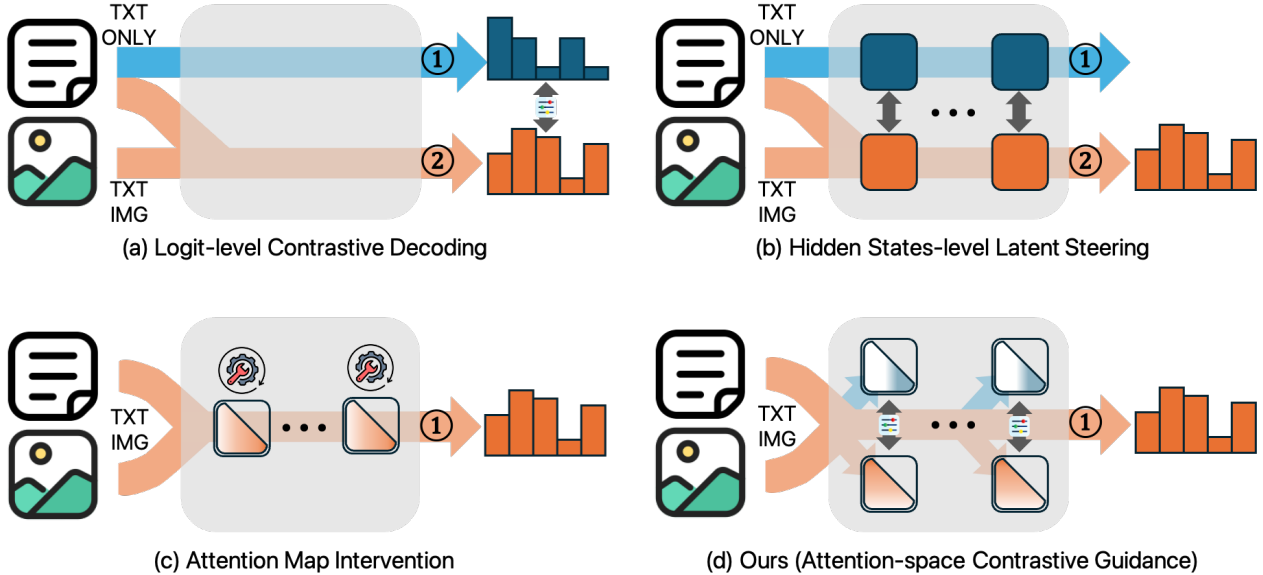


Figure 1. **Comparison of inference-time strategies for mitigating LVLM hallucinations.** (a) Logit-level contrastive decoding, (b) hidden-state-level latent steering, (c) attention map intervention, and (d) the proposed Attention-space Contrastive Guidance (ACG).

attention-level biases where hallucinations originate. Second, they typically require multiple forward passes, leading to significant computational overhead and limiting their applicability in real-time or large-scale settings. A few recent methods intervene on attention maps directly, but these approaches often rely on pattern-specific heuristics and lack a clear, unified objective that explicitly ties attention manipulation to image-grounded faithfulness [4, 9–11, 21, 34, 38].

In this paper, we propose *Attention-space Contrastive Guidance* (ACG), a training-free, single-pass guidance mechanism that operates directly within the self-attention layers of an LVLM. Rather than applying a single global correction at the output layer, ACG performs contrastive guidance in attention space by constructing image–text (image-conditioned) and text-only (unconditional) attention paths within a single forward pass and using their difference to steer attention toward visual evidence as decoding unfolds. We further characterize the approximation bias introduced by masking-based construction of the text-only path and apply an orthogonalized correction that isolates the purely visual contribution. This attention-space formulation provides fine-grained, interpretable control over cross-modal alignment while remaining computationally efficient, achieving comparable or better hallucination reduction than prior multi-pass contrastive decoding methods.

Our main contributions are as follows:

- We formulate LVLM hallucination mitigation as contrastive guidance in attention space and instantiate it as Attention-space Contrastive Guidance (ACG), a training-free single-pass mechanism that constructs image-

conditioned and approximate text-only attention paths within each attention layer and performs attention-level correction of cross-modal biases during decoding.

- To compensate for the approximation bias induced by the masking-based approximation of the unconditional path in attention space, we introduce an orthogonalized correction that cleanly separates visual contributions from language priors.
- We demonstrate that ACG consistently improves faithfulness on standard hallucination benchmarks, including CHAIR and POPE, while achieving comparable or better hallucination reduction with up to  $2\times$  lower inference latency than prior training-free logit-level guidance baselines.

## 2. Related Work

### 2.1. LVLMs and Hallucinations

Large vision–language models (LVLMs) have shown remarkable capabilities in integrating vision and language and have been evaluated on a wide range of multimodal benchmarks [1, 2, 6, 15, 19, 37]. However, their practical deployment is hindered by hallucinations, where models generate text that is inconsistent with the visual input. This phenomenon, ranging from describing nonexistent objects to misstating attributes or relations, is often attributed to an imbalance in which the model’s powerful language priors override the actual visual evidence [3, 12, 17, 23, 24]. Mitigating this failure of image-grounded generation has therefore become a central goal of recent work on LVLM reli-

ability and evaluation, spanning training-based fine-tuning, decoding-time guidance, and attention-level interventions.

## 2.2. Controlled Generation in LVLMs

Our work frames hallucination mitigation as a controlled generation problem, aligning with several paradigms for steering generative models at inference time. Contrastive decoding (CD), proposed for language models [5, 16], steers generation by contrasting logits from a large model with those from a smaller model, and has been adapted to vision–language models to mitigate hallucinations [13, 14, 22, 30, 31], for example via visual contrastive decoding (VCD) [14]. Similarly, classifier-free guidance (CFG) [7, 25], originating in diffusion models, steers generation by combining conditional and unconditional forward passes with a guidance weight to amplify features consistent with the conditioning signal, and this concept has been applied to LVLMs at the logit level [29, 35, 36]. These logit-level methods (visualized in Figure 1 (a)) are computationally costly, as they require two separate forward passes and operate only at the output layer. Finally, latent steering (Figure 1 (b)) intervenes directly on the model’s hidden states (representations), an active line of work in LLMs [27] that has been extended to VLMs [18, 20, 26, 32], typically by adding a precomputed “steering vector” to the residual stream.

Our method, ACG, connects but also differs from these lines of work. Unlike CD- or CFG-based methods, which require multiple forward passes, ACG constructs image-conditioned and approximate text-only paths inside the self-attention layers of a single forward pass. Compared to latent steering, which generally utilizes a static steering vector, ACG derives a token-dependent steering direction on the fly from the contrast between image-conditioned and text-only attention outputs, as illustrated in Figure 1 (d).

## 2.3. Attention-based Interventions in LVLMs

A complementary line of work investigates LVLM failures through the lens of the attention mechanism, providing evidence that attention-level biases are tightly coupled with hallucinations and other vision-centric errors [4, 9, 34, 38]. Prior studies have reported phenomena such as “text inertia” (hallucinations persisting even without visual input) [21], fading or noisy visual attention as generation progresses [10], and “visual attention sinks” [11] or specialized “hallucination heads” [34]. However, current attention-based interventions motivated by these observations (Figure 1 (c)) remain fragmented and largely heuristic, with each method targeting a specific empirical pattern or relying on additional components such as offline causal analysis to pre-identify heads.

ACG takes a step toward bridging this gap by casting hallucination mitigation as attention-space contrastive guid-

ance. We define an explicit conditional–unconditional contrast at every attention layer and derive a geometric correction that separates visual contributions from language priors, together providing a unified, objective-driven alternative to prior heuristic attention interventions.

## 3. Method

We propose **Attention-space Contrastive Guidance** (ACG), a training-free, inference-time guidance mechanism for mitigating hallucinations in large vision–language models (LVLMs). This section first introduces the contrastive formulation in attention space, then describes our single-pass approximation of the unconditional path and the associated orthogonalized correction.

### 3.1. Preliminaries

**Architecture.** We consider LVLMs composed of a vision encoder, a projector, and a LLaMA-style language decoder. Given an image  $I$  and a text prompt, the vision encoder and projector yield visual embeddings  $X_v = [x_1^{(v)}, \dots, x_{n_v}^{(v)}]$  in the language embedding space. The decoder input is composed of system tokens  $X_s = [x_1^{(s)}, \dots, x_{n_s}^{(s)}]$ , visual tokens  $X_v$ , user query tokens  $X_q = [x_1^{(q)}, \dots, x_{n_q}^{(q)}]$ , and previously generated response tokens  $X_{<t} = [x_1, \dots, x_{t-1}]$ . The complete multimodal context is

$$X_c = \text{concat}(X_s, X_v, X_q, X_{<t}), \quad (1)$$

with total sequence length  $n = n_s + n_v + n_q + (t-1)$ .

**Autoregressive decoding.** At generation step  $t$ , the LVLM predicts the next token via

$$x_t \sim p_\theta(x_t | X_c) = \text{softmax}(H(h_{\text{current}}^{(L)})), \quad (2)$$

where  $h_{\text{current}}^{(L)}$  denotes the last-layer hidden state corresponding to the current decoding position and  $H$  is the output projection to logits.

### 3.2. Attention-space Contrastive Guidance

Hallucinations often arise when an LVLM’s language priors dominate over its visual evidence. Recent work [34] indicates that this failure originates primarily within multi-head attention (MHA) modules rather than MLPs. Thus, ACG intervenes directly at the source of cross-modal interaction, operating on the *attention output* rather than the final logits as in logit-level contrastive methods [14, 21, 25].

At each decoding step, we apply ACG to the current response token, i.e., the last text token in the sequence. For this query token  $q$ , we define two attention outputs:

- $O_{\text{cond}}$ : the *conditional* output, where  $q$  attends to all keys.
- $O_{\text{uncond}}$ : the *text-only (unconditional)* output, representing the model’s behavior without visual conditioning.

---

**Algorithm 1** Attention-space Contrastive Guidance (ACG) in Self-attention Blocks (LLaMA Version)

---

**Input:** Weights  $W_Q, W_K, W_V, W_O$ , hidden state  $H^{(l-1)}$ , and scaling factor  $\gamma$   
**Output:** Updated hidden state  $H^{(l)}$

▷ Pre-normalization

- 1:  $\tilde{H} \leftarrow \text{RMSNorm}(H^{(l-1)})$
- 2:  $Q \leftarrow \tilde{H}W_Q, K \leftarrow \tilde{H}W_K, V \leftarrow \tilde{H}W_V$
- ▷ Conditional and approximate text-only outputs
- 3:  $S \leftarrow \frac{QK^\top}{\sqrt{d_k}}$
- 4:  $A_{\text{cond}} \leftarrow \text{softmax}(S), O_{\text{cond}} \leftarrow A_{\text{cond}}V$
- ▷ Construct mask  $M$
- 5: Let query  $i^*$  be the index of the last text token.
- 6:  $M_{i^*j} \leftarrow -\infty$  if key  $j$  is visual;  $M_{ij} \leftarrow 0$  otherwise
- 7:  $A_{\text{uncond}} \leftarrow \text{softmax}(S + M), O_{\text{uncond}} \leftarrow A_{\text{uncond}}V$
- ▷ Contrastive correction with orthogonalization
- 8:  $\Delta O \leftarrow O_{\text{cond}} - O_{\text{uncond}}$
- 9:  $u \leftarrow \frac{O_{\text{uncond}}}{\|O_{\text{uncond}}\|_2 + \epsilon}$
- 10:  $\Delta O_\perp \leftarrow \Delta O - \langle \Delta O, u \rangle u$
- 11:  $O_{\text{final}} \leftarrow O_{\text{cond}} + \gamma \cdot \Delta O_\perp$
- ▷ Output projection and residual
- 12:  $Z \leftarrow O_{\text{final}}W_O$
- 13:  $H_{\text{attn}}^{(l)} \leftarrow H^{(l-1)} + Z$
- 14:  $H^{(l)} \leftarrow H_{\text{attn}}^{(l)} + \text{FFN}(\text{RMSNorm}(H_{\text{attn}}^{(l)}))$
- 15: **return**  $H^{(l)}$

---

The guided output is given by the contrastive interpolation

$$O_{\text{final}} = O_{\text{cond}} + \gamma \cdot (O_{\text{cond}} - O_{\text{uncond}}), \quad (3)$$

where  $\gamma$  controls the strength of guidance.

However, if we compute  $O_{\text{uncond}}$  using a separate forward pass with non-image input, as in prior work [18, 21], this guidance step requires an additional pass and roughly doubles inference time. ACG avoids this cost by *approximating* the unconditional path within a single forward pass using a masking strategy.

Specifically, we compute the query, key, and value matrices  $(Q, K, V)$  once per layer. The conditional attention output is obtained as:

$$A_{\text{cond}} = \text{softmax}\left(\frac{QK^\top}{\sqrt{d_k}}\right), \quad O_{\text{cond}} = A_{\text{cond}}V \quad (4)$$

To approximate the text-only (unconditional) path for the current response token, we reuse the score matrix  $S = \frac{QK^\top}{\sqrt{d_k}}$  but apply a binary mask  $M$  that suppresses attention to visual keys from the last text query. Concretely, for the last text token index  $i^*$ , we set  $M_{i^*j} = -\infty$  if key  $j$  is

visual and  $M_{ij} = 0$  otherwise, and define

$$A_{\text{uncond}} = \text{softmax}(S + M), \quad O_{\text{uncond}} = A_{\text{uncond}}V \quad (5)$$

This masking operation effectively removes visual contributions for the current text query, simulating an image-agnostic state while preserving the same computational graph and reusing all intermediate states. We expect this single-pass approximation to capture the language-biased behavior that underlies hallucination.

### 3.3. Textual Orthogonalization

While efficient, the masking approximation introduces an inherent *approximation bias*: the masked  $O_{\text{uncond}}$  does not perfectly match a true image-absent forward pass. Two major factors contribute to this bias:

1. **Contextual leakage.** Earlier layers  $(1, \dots, l-1)$  already inject visual context into  $Q, K_{\text{text}}$ , and  $V_{\text{text}}$ , so masking visual keys at layer  $l$  cannot remove accumulated visual information.
2. **Softmax redistribution.** When visual keys are masked, attention mass that would target visual tokens is redistributed to text tokens, amplifying text–text correlations and changing language priors.

As a result, the naive guidance vector  $\Delta O = O_{\text{cond}} - O_{\text{uncond}}$  mixes true visual correction with text-induced distortion, which can degrade response quality at high guidance scales  $\gamma$ .

To address this, ACG applies **textual orthogonalization**, a geometric correction that disentangles the visual signal from textual bias. We treat  $O_{\text{uncond}}$  as defining the principal textual direction and remove from  $\Delta O$  any component aligned with it.

First, we define the unit direction

$$u = \frac{O_{\text{uncond}}}{\|O_{\text{uncond}}\|_2 + \epsilon} \quad (6)$$

where  $\epsilon$  ensures numerical stability. We then project  $\Delta O$  onto the subspace orthogonal to  $u$ :

$$\Delta O_\perp = \Delta O - \langle \Delta O, u \rangle u \quad (7)$$

This operation removes components parallel to the text-only path, isolating the visually grounded correction. The final guided output is

$$O_{\text{final}} = O_{\text{cond}} + \gamma \cdot \Delta O_\perp \quad (8)$$

This purified correction amplifies the visual contribution while preventing runaway drift along the textual direction, improving the stability of guidance at higher  $\gamma$ . We apply this correction at every decoding step across all self-attention layers used by ACG, and the full procedure is summarized in Algorithm 1.

Table 1. **POPE results (%) on LLaVA-1.5, MiniGPT-4, and Qwen-VL**. We report overall average accuracy (Avg.) as well as accuracy (Acc.), precision (Prec.), recall (Rec.), and F1 under the *Random*, *Popular*, and *Adversarial* settings. **Bold** numbers indicate the best performance in each column.

Model	Method	Avg.	Random				Popular				Adversarial			
			Acc.	Acc.	Prec.	Rec.	F1	Acc.	Prec.	Rec.	F1	Acc.	Prec.	Rec.
LLaVA [19]	Regular	84.83	<b>89.37</b>	89.66	89.00	<b>89.33</b>	86.00	84.05	88.87	86.39	79.13	74.39	88.87	80.98
	VCD [14]	85.38	88.63	91.96	84.67	88.16	85.97	86.93	84.67	85.78	81.53	79.67	84.67	82.09
	PAI [21]	84.91	89.30	89.54	89.00	89.27	86.13	84.26	88.87	<b>86.50</b>	79.30	74.59	88.87	81.11
	VISTA [18]	83.03	88.25	87.31	<b>90.33</b>	88.79	84.10	80.21	<b>90.53</b>	85.06	76.73	70.93	<b>90.60</b>	79.57
	Ours	<b>86.03</b>	88.30	<b>95.92</b>	80.00	87.24	<b>86.57</b>	<b>92.22</b>	79.87	85.60	<b>83.23</b>	<b>85.63</b>	79.87	<b>82.65</b>
MiniGPT-4 [37]	Regular	76.31	82.47	<b>89.27</b>	73.80	80.80	75.00	75.48	74.07	74.76	71.47	70.41	74.07	72.19
	PAI	76.59	82.23	88.53	74.07	80.65	<b>75.80</b>	<b>76.62</b>	74.27	75.42	71.73	<b>70.69</b>	74.27	72.43
	VISTA	76.19	82.30	87.40	<b>76.73</b>	<b>81.72</b>	75.10	74.18	<b>77.00</b>	<b>75.56</b>	71.17	69.07	<b>76.67</b>	72.67
	Ours	<b>76.70</b>	<b>82.70</b>	88.90	74.73	81.20	75.50	75.76	75.00	75.38	<b>71.90</b>	70.62	75.00	<b>72.74</b>
Qwen-VL [2]	Regular	85.51	86.67	<b>98.50</b>	74.47	84.81	85.80	<b>96.29</b>	74.47	83.98	84.07	<b>92.23</b>	74.40	82.36
	VCD	86.77	88.83	94.64	82.33	88.06	87.23	90.98	82.67	86.62	<b>84.23</b>	85.44	82.53	<b>83.96</b>
	Ours	<b>86.98</b>	<b>89.17</b>	93.81	<b>83.87</b>	<b>88.56</b>	<b>88.23</b>	91.89	<b>83.87</b>	<b>87.70</b>	83.53	83.27	<b>83.93</b>	83.60

## 4. Experiments

### 4.1. Experimental Settings

**Datasets and Benchmarks.** We evaluate on two widely used hallucination benchmarks, POPE [17] and CHAIR [24], built on MS COCO. For further evaluation, we choose MMHal-Bench [28]. POPE measures binary yes/no object existence, while CHAIR evaluates object hallucinations in free-form captions. MMHal-Bench consists of 96 image–question pairs that probe object and attribute-level inconsistencies. Model responses’ alignment with ground-truth answers is evaluated by GPT-4.

**Baselines.** We compare ACG against three representative inference-time approaches: (i) logit-level contrastive decoding (VCD [14]), (ii) logit-level classifier-free guidance with attention intervention (PAI [21]), and (iii) latent steering (VISTA [18]). This covers output-logit, latent-space, and attention-space interventions for LVLMs. All methods use greedy decoding with the same maximum generation length per benchmark.

**Models.** We consider three LVLMs with diverse language backbones and vision-language connectors: LLaVA-1.5 [19], MiniGPT-4 [37], and Qwen-VL [2]. For each baseline, we only evaluate on LVLMs officially supported by the authors’ public implementations to avoid unfair or unstable re-implementations.

**Implementation Details.** To demonstrate our method’s generability among tasks, we set  $\gamma$  to 2.4 for LLaVA-1.5 [19], 0.3 for MiniGPT-4 [37], 1.4 for Qwen-VL [2] for all experiments unless explicitly stated otherwise. For a consistent and comparative analysis, we set greedy decoding as default.

Table 2. **CHAIR results (%) on LLaVA-1.5 and MiniGPT-4**. **Bold** indicates the best CHAIR performance and underlines indicate the second-best in each column.

Model	Method	Max Tokens	128			64		
			CHAIR <sub>s</sub>	CHAIR <sub>i</sub>	F1	CHAIR <sub>s</sub>	CHAIR <sub>i</sub>	F1
LLaVA [19]	Regular	56.2	18.3	70.6	25.2	8.3	68.5	
	VCD	55.0	17.0	72.5	27.2	8.8	70.0	
	PAI	<u>25.6</u>	<u>7.6</u>	75.9	<b>13.8</b>	<b>4.5</b>	72.4	
	VISTA	31.0	10.5	76.6	23.6	7.6	74.3	
	Ours	<b>21</b>	<b>4.8</b>	74.4	<u>16.8</u>	<b>4.5</b>	72.8	
MiniGPT-4 [37]	Regular	35.0	10.8	69.8	24.8	8.2	69.3	
	PAI	22.8	8.1	71.4	19.8	6.9	71.0	
	VISTA	18.8	<u>5.9</u>	71.0	<u>15.8</u>	<u>5.5</u>	70.2	
	Ours	<b>10.8</b>	<b>3.3</b>	68.0	<b>11.2</b>	<b>4.2</b>	67.9	

### 4.2. Experimental Results

**Results on POPE.** Experiment results on POPE under the random, popular, adversarial settings and total average scores are shown in Tab. 1. Our approach outperforms baselines on average score. Especially, our approach shows notable increase in adversarial set on LLaVA-1.5 and MiniGPT-4, which is considered the most difficult set as negative samples are semantically or statistically related to objects that do appear in the image. It demonstrates that our approach effectively mitigates hallucination, by generating response without reliance on language prior.

**Results on CHAIR.** Experiment results on open-ended generation with CHAIR are shown in Tab. 2. We report sentence-level hallucination rate (CHAIR<sub>s</sub>), instance-level hallucination rate (CHAIR<sub>i</sub>), and F1 score. We report results with  $\text{max\_new\_tokens} \in \{64, 128\}$  to disentangle the effect of caption length from hallucination reduction.

Across both models and length budgets, ACG consistently achieves the lowest instance-level hallucination

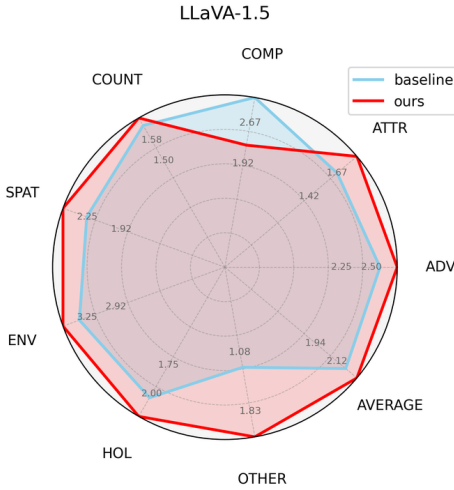
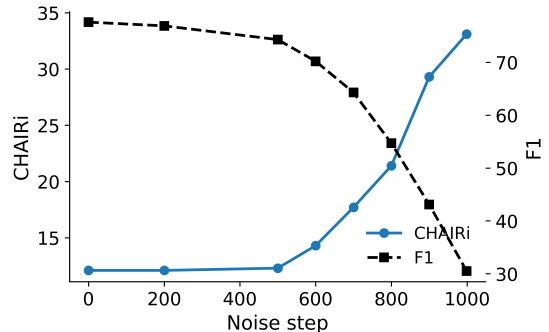


Figure 2. **MMHal-Bench results on LLaVA-1.5.** The radar chart reports GPT-4-judged hallucination scores across eight categories.

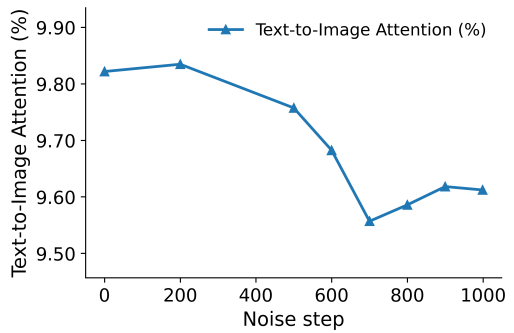
( $\text{CHAIR}_i$ ), indicating the strongest suppression of object hallucinations. On LLaVA-1.5, ACG reduces  $\text{CHAIR}_i$  to 4.8 and  $\text{CHAIR}_s$  to 21.0 under the 128-token budget while keeping F1 close to the best baseline, and under the 64-token budget it matches the best  $\text{CHAIR}_i$  with comparable  $\text{CHAIR}_s$  and F1. On MiniGPT-4, ACG attains the best  $\text{CHAIR}_s$  and  $\text{CHAIR}_i$  in both length settings with only a mild drop in F1, showing that attention-space guidance substantially reduces hallucinations while largely preserving object-level fidelity.

ACG achieves the best performance under the 128-token setting with only a minimal gap from the 64-token case, suggesting that it effectively alleviates the additional hallucinations that typically emerge over longer generation steps.

**Results on MMHal-Bench.** To assess the effect of our proposed method on logical reasoning and complex visual understanding, we conduct comparison between the baseline and our model on the LLaVA-1.5 architecture, as illustrated in Fig. 2. The radar chart reports hallucination-related metrics across eight categories: object attributes (ATTR), adversarial objects (ADV), comparisons (COMP), counting (COUNT), spatial relations (SPAT), environmental inferences (ENV), holistic descriptions (HOL), and others (OTHER), where higher scores indicate better factual alignment and reduced hallucination. Overall, our method consistently outperforms the baseline on average score, with higher scores across nearly all categories. It confirms that our approach enhances robustness against hallucination while maintaining general performance across diverse categories. Note that, for this evaluation, we adopt  $\gamma = 2.0$ , as a slightly weaker weighting yielded more stable behavior in this controlled comparison.



(a) Noisy images increase Hallucinations



(b) Text-to-Image Attention decreases with Visual Info Loss

Figure 3. **Validation of the masked-unconditional approximation.** (a) Increasing Gaussian noise (visual information loss) raises hallucination ( $\text{CHAIR}_i$ ) and worsens fidelity (F1). (b) Mean text-to-image (T2I) attention ratio shows an overall downward trend as visual information is lost.

## 5. Analysis

In this section, we present analyses that validate our Attention-space Contrastive Guidance (ACG). We first justify our single-pass approximation and show that textual orthogonalization is crucial for improving faithfulness while preserving object-level fidelity. We then analyze parameter sensitivity to provide a principled basis for configuring ACG, and finally quantify the efficiency gains of our approach.

### 5.1. Justifying the Masked Unconditional Path

ACG relies on a single-pass surrogate of the text-only path,  $O_{\text{uncond}}^{\text{mask}}$ , obtained by masking visual keys in attention (Sec. 3). We validate that this surrogate faithfully reflects the ungrounded, language-prior regime that emerges when visual evidence is weak or absent.

**Protocols.** We progressively degrade the input image by adding Gaussian noise (noise step  $\in \{0, \dots, 999\}$ ), run the vanilla LLaVA model (no guidance), and measure: (i) instance-level hallucination ( $\text{CHAIR}_i$ ), (ii) object-level fidelity (F1), and (iii) mean text-to-image (T2I) attention ra-

Table 3. **Ablation at matched F1.** At comparable object-level fidelity, ACG (w/ Ortho) yields lower hallucinations than ACG (w/o Ortho). Lower is better for  $\text{CHAIR}_s/\text{CHAIR}_i$ .

Method	$\gamma$	$\text{F1} \uparrow$	$\text{CHAIR}_s \downarrow$	$\text{CHAIR}_i \downarrow$
ACG (w/ Ortho)	2.1	<b>77.6</b>	<b>34.2</b>	<b>7.6</b>
ACG (w/o Ortho)	1.2	77.4	38.8	9.7
ACG (w/ Ortho)	2.4	<b>74.4</b>	<b>21.0</b>	<b>4.8</b>
ACG (w/o Ortho)	1.3	74.0	30.4	8.8

ratio, averaged across all generated tokens, layers, and heads.

**Finding 1: Visual Information Loss Correlates with Hallucination.** As shown in Fig. 3(a), increasing noise correlates with a catastrophic loss of faithfulness:  $\text{CHAIR}_i$  (hallucinations) rises sharply from 12.1 to 33.1, while F1 (fidelity) collapses from 77.6 to 30.5, with a pronounced knee near the 600-step mark. Consistent with prior observations that visual corruption exacerbates hallucination [20], this trend confirms our hypothesis: removing visual evidence pushes the model toward a text-biased, high-hallucination regime. This supports the view that the “language-only” state (the limit of this trend) is the correct target for intervention.

**Finding 2: The Model Naturally Gates Uninformative Inputs.** Fig. 3(b) provides mechanistic evidence. As noise is added, the model’s average T2I attention shows a clear downward trend, dropping from 9.82% to a minimum of 9.56% at the 700-step mark. This demonstrates that the model’s natural response to information-poor inputs is to reduce visual grounding. We note a minor rebound in T2I attention after this 700-step tipping point. However, this non-monotonic behavior does not contradict our finding. In the same region (700  $\rightarrow$  999 steps), faithfulness continues to deteriorate rapidly (Fig. 3a), indicating that the model remains in an ungrounded, high-hallucination regime despite the small attention rebound.

**Summary.** Taken together, degrading visual inputs induces (i) rising hallucinations and collapsing fidelity, and (ii) a primary trend of reduced T2I attention. These findings justify our use of  $O_{\text{uncond}}^{\text{mask}}$ : it serves as a principled, single-pass proxy for the model’s *natural* response (gating T2I attention) and directly targets the *source* of hallucinations (the language-only state).

## 5.2. Effect of Textual Orthogonalization

Our primary component, textual orthogonalization, is designed to correct the approximation bias introduced by the masking-based construction of  $O_{\text{uncond}}^{\text{mask}}$  that enables our single-pass algorithm. We hypothesize that this bias contaminates the naive guidance vector  $\Delta O$ , so that reducing hallucinations comes at an unnecessarily large cost in object-level fidelity (CHAIR F1). To test this, we run a con-

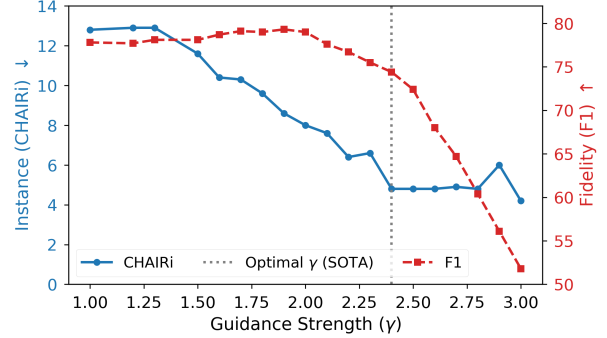


Figure 4. **Guidance-scale trade-off on LLaVA-1.5 (CHAIR, max 128).** Increasing  $\gamma$  lowers instance hallucination ( $\text{CHAIR}_i$ , blue; left axis) but eventually reduces object-level fidelity (F1, red; right axis). The dotted line marks the canonical setting  $\gamma=2.4$ .

trolled ablation comparing **ACG with Ortho** against a naive **ACG without Ortho**. We choose guidance scales that yield similar F1 and then compare sentence-level and instance-level faithfulness ( $\text{CHAIR}_s$ ,  $\text{CHAIR}_i$ ).

Table 3 provides strong evidence for the benefit of orthogonalization. At the  $\approx 74$  F1 operating point, ACG (w/ Ortho) attains  $1.8 \times$  lower  $\text{CHAIR}_i$  ( $8.8 \rightarrow 4.8$ ) and  $1.4 \times$  lower  $\text{CHAIR}_s$  ( $30.4 \rightarrow 21.0$ ) than ACG (w/o Ortho). Thus, removing the text-aligned component of  $\Delta O$  allows us to substantially reduce hallucinations while keeping F1 nearly unchanged, leading to state-of-the-art faithfulness among evaluated inference-time methods.

## 5.3. Simplicity and Parameter Analysis

ACG exposes a single hyperparameter, the guidance scale  $\gamma$ , and by default applies guidance to all layers (no layer-selection tuning). We characterize how  $\gamma$  continuously trades off faithfulness, fidelity, and length.

**Guidance scale trade-off.** Figure 4 summarizes a sweep over  $\gamma \in [1.0, 3.0]$  on CHAIR (max 128). As  $\gamma$  increases, instance hallucination ( $\text{CHAIR}_i$ ) decreases from 12.8 at  $\gamma=1.0$  to around 5 near  $\gamma=2.4$ , while object-level fidelity (F1) stays in the high 70s up to this range. Beyond  $\gamma \approx 2.4$ , F1 drops sharply and captions become overly short. We therefore adopt  $\gamma=2.4$  as a canonical operating point, which achieves strong hallucination reduction ( $\text{CHAIR}_i=4.8$ ) while maintaining acceptable fidelity (F1=74.4) and reasonable caption length.

**Block-wise characterization.** While our default setup remains *All layers*, to understand where guidance is most effective, we partition the 32-layer decoder into four contiguous blocks and sweep  $\gamma$  for each block, reporting representative operating points in Table 4. Applying guidance to **Early** layers already yields substantial hallucination reduction at modest scales, while **All** layers attain the strongest reduction overall. In contrast, the other layer blocks require

Table 4. **Block-wise characterization on LLaVA-1.5 (CHAIR, max 128).** We report representative operating points along each curve.

Layer Block	$\gamma$	$\text{CHAIR}_i (\downarrow)$	$\text{F1} (\uparrow)$	$\text{Len} (\downarrow)$
<b>All (1-32)</b>	<b>2.4</b>	<b>4.8</b>	74.4	72.4
Early (1-8)	2.5	7.1	77.5	77.6
Early (1-8)	3.0	5.3	69.8	68.0
Early-Mid (9-16)	6.0	11.1	74.8	79.2
Early-Mid (9-16)	8.0	5.7	56.6	45.9
Mid-Late (17-24)	6.0	10.7	77.4	95.6
Mid-Late (17-24)	10.0	7.0	73.4	91.8
Late (25-32)	2.5	10.7	78.6	93.0
Late (25-32)	10.0	8.8	75.7	90.7

Table 5. **Efficiency vs. faithfulness on LLaVA-1.5 (CHAIR, max 128.)** All values are averages.

Method	Level	Passes	Per-image Latency (s) $\downarrow$	Per-word Latency (s) $\downarrow$	$\text{CHAIR}_i \downarrow$
Regular	-	1-pass	2.81 (1.00 $\times$ )	0.03	18.3
VCD	Logit	2-pass	5.54 (1.97 $\times$ )	0.06	17.0
PAI	Logit+Attn	2-pass	6.42 (2.28 $\times$ )	0.07	7.6
VISTA	Latent	3-pass	5.55 (1.98 $\times$ )	0.07	10.5
ACG-Fast	Attention	<b>1-pass</b>	<b>2.96 (1.05<math>\times</math>)</b>	<b>0.04</b>	7.3
ACG-Full	Attention	<b>1-pass</b>	3.34 (1.19 $\times$ )	0.05	<b>4.8</b>

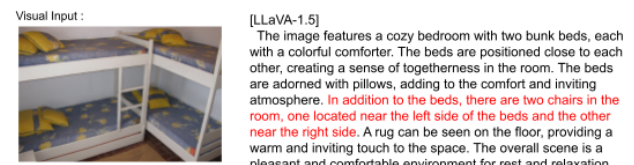
much larger  $\gamma$  to meaningfully influence the output yet deliver weaker gains. This indicates that cross-modal bias is most effectively corrected where text and vision first interact.

#### 5.4. Computational Efficiency

We measure average wall-clock latency per image and per word on CHAIR (max new tokens = 128, greedy decoding), using the same environment across methods.

Our goal is to compare *cost* (latency and number of forward passes) against *benefit* (faithfulness,  $\text{CHAIR}_i$ ). We report two canonical operating modes that keep ACG a *single-knob*, single-pass method: **ACG-Full** (guidance on all layers) for maximum faithfulness, and **ACG-Fast** (guidance on the first 8 layers) as a compute-conscious alternative. Both expose only the guidance scale  $\gamma$ ; no layer-selection hyperparameter is introduced.

Multi-pass baselines nearly double latency (1.97–2.28 $\times$ ), whereas ACG remains single-pass. **ACG-Full** achieves state-of-the-art faithfulness ( $\text{CHAIR}_i=4.8$ ) at only 1.19 $\times$  the vanilla cost, outperforming the 2-pass PAI (7.6) in both accuracy and speed. **ACG-Fast** retains most of the gains at near-vanilla cost (1.05 $\times$ ). These results justify using ACG-Full as the default and ACG-Fast as a compute-friendly alternative, without introducing any additional hyperparameters.



Query : Describe the image in detail.

[LLaVA-1.5]

The image features a cozy bedroom with two bunk beds, each with a colorful comforter. The beds are positioned close to each other, creating a sense of togetherness in the room. The beds are adorned with pillows, adding to the comfort and inviting atmosphere. In addition to the beds, there are two chairs in the room, one located near the left side of the beds and the other near the right side. A rug can be seen on the floor, providing a warm and inviting touch to the space. The overall scene is a pleasant and comfortable environment for rest and relaxation.

Visual Input :



Query : Is this photo taken in a restaurant, a kitchen, or anywhere else?

[Ours]

The image features a bedroom with two bunk beds, each with a blue and yellow pillow. The beds are placed on a brick floor, and the pillows are yellow. The beds are positioned next to each other, creating a cozy and comfortable sleeping arrangement.

[Ground Truth Answer]

This photo is taken outdoors, likely on a beach, where a man is cooking on a grill.

[LLaVA-1.5]

This photo is taken in a restaurant, as evidenced by the presence of a man cooking food on a grill and the presence of a dining table.

[Ours]

This photo is taken at a beach, where a man is cooking food on a grill.

Figure 5. **Qualitative Analysis.** Comparison between responses generated by LLaVA-1.5 and LLaVA-1.5 with ACG(Ours). Hallucinated/Wrong and accurate content is highlighted in red and blue.

#### 5.5. Qualitative Analysis

In Fig. 5, we compare the responses on MMHal-Bench between the LLaVA-1.5 model and LLaVA-1.5 with ACG. In the upper example, LLaVA-1.5 hallucinates in the later decoding stages, whereas LLaVA-1.5 with ACG avoids such hallucination and instead correctly mentions the “brick floor”. In the bottom example, LLaVA-1.5 shows an inaccurate scene interpretation and hallucination. In contrast, LLaVA-1.5 with ACG correctly identifies that “This photo is taken at a beach”, which matches with the ground truth answer. These qualitative examples validate that our method effectively suppresses hallucinations by preserving visual grounding and maintaining contextual accuracy throughout the generation process.

#### 6. Conclusion

In this paper, we proposed Attention-space Contrastive Guidance (ACG), a training-free, inference-time method for mitigating hallucinations in large vision–language models. ACG operates directly in self-attention layers by approximating a text-only path via masked visual keys and applying a textual orthogonalization step to isolate purely visual contributions geometrically. Experiments on CHAIR, POPE show that ACG attains state-of-the-art faithfulness while remaining single-pass and computationally efficient, outperforming prior multi-pass logit-level guidance methods in both accuracy and latency.

## References

- [1] Jean-Baptiste Alayrac, Jeff Donahue, Pauline Luc, Antoine Miech, Iain Barr, Yana Hasson, Karel Lenc, Arthur Mensch, Katie Millican, Malcolm Reynolds, Roman Ring, Eliza Rutherford, Serkan Cabi, Tengda Han, Zhitao Gong, Sina Samangoeei, Marianne Monteiro, Jacob Menick, Sebastian Borgeaud, Andrew Brock, Aida Nematzadeh, Sahand Sharifzadeh, Mikolaj Binkowski, Ricardo Barreira, Oriol Vinyals, Andrew Zisserman, and Karen Simonyan. Flamingo: a visual language model for few-shot learning, 2022. [1](#), [2](#)
- [2] Jinze Bai, Shuai Bai, Shusheng Yang, Shijie Wang, Sinan Tan, Peng Wang, Junyang Lin, Chang Zhou, and Jingren Zhou. Qwen-vl: A versatile vision-language model for understanding, localization, text reading, and beyond, 2023. [1](#), [2](#), [5](#)
- [3] Zechen Bai, Pichao Wang, Tianjun Xiao, Tong He, Zongbo Han, Zheng Zhang, and Mike Zheng Shou. Hallucination of multimodal large language models: A survey, 2025. [1](#), [2](#)
- [4] Shiqi Chen, Tongyao Zhu, Ruochen Zhou, Jinghan Zhang, Siyang Gao, Juan Carlos Niebles, Mor Geva, Junxian He, Jiajun Wu, and Manling Li. Why is spatial reasoning hard for vlms? an attention mechanism perspective on focus areas, 2025. [2](#), [3](#)
- [5] Yung-Sung Chuang, Yujia Xie, Hongyin Luo, Yoon Kim, James Glass, and Pengcheng He. Dola: Decoding by contrasting layers improves factuality in large language models, 2024. [3](#)
- [6] Wenliang Dai, Junnan Li, Dongxu Li, Anthony Meng Huat Tiong, Junqi Zhao, Weisheng Wang, Boyang Li, Pascale Fung, and Steven Hoi. Instructblip: Towards general-purpose vision-language models with instruction tuning, 2023. [1](#), [2](#)
- [7] Jonathan Ho and Tim Salimans. Classifier-free diffusion guidance, 2022. [3](#)
- [8] Chaoya Jiang, Haiyang Xu, Mengfan Dong, Jiaxing Chen, Wei Ye, Ming Yan, Qinghao Ye, Ji Zhang, Fei Huang, and Shikun Zhang. Hallucination augmented contrastive learning for multimodal large language model, 2024. [1](#)
- [9] Zhangqi Jiang, Junkai Chen, Beier Zhu, Tingjin Luo, Yankun Shen, and Xu Yang. Devils in middle layers of large vision-language models: Interpreting, detecting and mitigating object hallucinations via attention lens, 2025. [2](#), [3](#)
- [10] Mingu Jung, Saehyung Lee, Eunji Kim, and Sungroh Yoon. Visual attention never fades: Selective progressive attention recalibration for detailed image captioning in multimodal large language models, 2025. [3](#)
- [11] Seil Kang, Jinyeong Kim, Junhyeok Kim, and Seong Jae Hwang. See what you are told: Visual attention sink in large multimodal models, 2025. [2](#), [3](#)
- [12] Prannay Kaul, Zhizhong Li, Hao Yang, Yonatan Dukler, Ashwin Swaminathan, C. J. Taylor, and Stefano Soatto. Throne: An object-based hallucination benchmark for the free-form generations of large vision-language models, 2025. [1](#), [2](#)
- [13] Yi-Lun Lee, Yi-Hsuan Tsai, and Wei-Chen Chiu. Delve into visual contrastive decoding for hallucination mitigation of large vision-language models, 2024. [3](#)
- [14] Sicong Leng, Hang Zhang, Guanzheng Chen, Xin Li, Shijian Lu, Chunyan Miao, and Lidong Bing. Mitigating object hallucinations in large vision-language models through visual contrastive decoding. In *Proceedings of the IEEE/CVF Conference on Computer Vision and Pattern Recognition (CVPR)*, pages 13872–13882, 2024. [1](#), [3](#), [5](#), [2](#)
- [15] Junnan Li, Dongxu Li, Silvio Savarese, and Steven Hoi. Blip-2: Bootstrapping language-image pre-training with frozen image encoders and large language models, 2023. [1](#), [2](#)
- [16] Xiang Lisa Li, Ari Holtzman, Daniel Fried, Percy Liang, Jason Eisner, Tatsunori Hashimoto, Luke Zettlemoyer, and Mike Lewis. Contrastive decoding: Open-ended text generation as optimization. In *Proceedings of the 61st Annual Meeting of the Association for Computational Linguistics (Volume 1: Long Papers)*, pages 12286–12312, Toronto, Canada, 2023. Association for Computational Linguistics. [3](#)
- [17] Yifan Li, Yifan Du, Kun Zhou, Jinpeng Wang, Xin Zhao, and Ji-Rong Wen. Evaluating object hallucination in large vision-language models. In *Proceedings of the 2023 Conference on Empirical Methods in Natural Language Processing*, pages 292–305, Singapore, 2023. Association for Computational Linguistics. [1](#), [2](#), [5](#)
- [18] Zhuowei Li, Haizhou Shi, Yunhe Gao, Di Liu, Zhenting Wang, Yuxiao Chen, Ting Liu, Long Zhao, Hao Wang, and Dimitris N. Metaxas. The hidden life of tokens: Reducing hallucination of large vision-language models via visual information steering. In *Proceedings of the 42nd International Conference on Machine Learning*, pages 35799–35819. PMLR, 2025. [3](#), [4](#), [5](#), [2](#)
- [19] Haotian Liu, Chunyuan Li, Yuheng Li, and Yong Jae Lee. Improved baselines with visual instruction tuning. In *Proceedings of the IEEE/CVF Conference on Computer Vision and Pattern Recognition (CVPR)*, pages 26296–26306, 2024. [1](#), [2](#), [5](#)
- [20] Sheng Liu, Haotian Ye, Lei Xing, and James Zou. Reducing hallucinations in vision-language models via latent space steering, 2024. [3](#), [7](#)
- [21] Shi Liu, Kecheng Zheng, and Wei Chen. Paying more attention to image: A training-free method for alleviating hallucination in lvms, 2024. [1](#), [2](#), [3](#), [4](#), [5](#)
- [22] Woohyeon Park, Woojin Kim, Jaeik Kim, and Jaeyoung Do. Second: Mitigating perceptual hallucination in vision-language models via selective and contrastive decoding, 2025. [1](#), [3](#)
- [23] Suzanne Petryk, David M. Chan, Anish Kachinthaya, Haodi Zou, John Canny, Joseph E. Gonzalez, and Trevor Darrell. Aloha: A new measure for hallucination in captioning models, 2024. [2](#)
- [24] Anna Rohrbach, Lisa Anne Hendricks, Kaylee Burns, Trevor Darrell, and Kate Saenko. Object hallucination in image captioning. In *Proceedings of the 2018 Conference on Empirical Methods in Natural Language Processing*, pages 4035–4045, Brussels, Belgium, 2018. Association for Computational Linguistics. [1](#), [2](#), [5](#)

- [25] Guillaume Sanchez, Honglu Fan, Alexander Spangher, Elad Levi, Pawan Sasanka Ammanamanchi, and Stella Biderman. Stay on topic with classifier-free guidance, 2023. 3
- [26] Jingran Su, Jingfan Chen, Hongxin Li, Yuntao Chen, Li Qing, and Zhaoxiang Zhang. Activation steering decoding: Mitigating hallucination in large vision-language models through bidirectional hidden state intervention. In *Proceedings of the 63rd Annual Meeting of the Association for Computational Linguistics (Volume 1: Long Papers)*, pages 12964–12974, Vienna, Austria, 2025. Association for Computational Linguistics. 3
- [27] Nishant Subramani, Nivedita Suresh, and Matthew Peters. Extracting latent steering vectors from pretrained language models. In *Findings of the Association for Computational Linguistics: ACL 2022*, pages 566–581, Dublin, Ireland, 2022. Association for Computational Linguistics. 3
- [28] Zhiqing Sun, Sheng Shen, Shengcao Cao, Haotian Liu, Chunyuan Li, Yikang Shen, Chuang Gan, Liangyan Gui, Yu-Xiong Wang, Yiming Yang, Kurt Keutzer, and Trevor Darrell. Aligning large multimodal models with factually augmented RLHF. In *Findings of the Association for Computational Linguistics: ACL 2024*, pages 13088–13110, Bangkok, Thailand, 2024. Association for Computational Linguistics. 1, 5
- [29] David Wan, Jaemin Cho, Elias Stengel-Eskin, and Mohit Bansal. Contrastive region guidance: Improving grounding in vision-language models without training, 2024. 3
- [30] Zifu Wan, Ce Zhang, Silong Yong, Martin Q. Ma, Simon Stepputtis, Louis-Philippe Morency, Deva Ramanan, Katia Sycara, and Yaqi Xie. Only: One-layer intervention sufficiently mitigates hallucinations in large vision-language models, 2025. 3
- [31] Xintong Wang, Jingheng Pan, Liang Ding, and Chris Biemann. Mitigating hallucinations in large vision-language models with instruction contrastive decoding, 2024. 1, 3
- [32] Junfei Wu, Yue Ding, Guofan Liu, Tianze Xia, Ziyue Huang, Dianbo Sui, Qiang Liu, Shu Wu, Liang Wang, and Tieniu Tan. SHARP: Steering hallucination in LVLMs via representation engineering. In *Proceedings of the 2025 Conference on Empirical Methods in Natural Language Processing*, pages 14357–14372, Suzhou, China, 2025. Association for Computational Linguistics. 3
- [33] Jiulong Wu, Zhengliang Shi, Shuaiqiang Wang, Jizhou Huang, Dawei Yin, Lingyong Yan, Min Cao, and Min Zhang. Mitigating hallucinations in large vision-language models via entity-centric multimodal preference optimization, 2025. 1
- [34] Tianyun Yang, Ziniu Li, Juan Cao, and Chang Xu. Mitigating hallucination in large vision-language models via modular attribution and intervention. In *The Thirteenth International Conference on Learning Representations*, 2025. 2, 3
- [35] Yuechen Zhang, Shengju Qian, Bohao Peng, Shu Liu, and Jiaya Jia. Prompt highlighter: Interactive control for multimodal llms, 2024. 3
- [36] Linxi Zhao, Yihe Deng, Weitong Zhang, and Quanquan Gu. Mitigating object hallucination in large vision-language models via image-grounded guidance, 2025. 3
- [37] Deyao Zhu, Jun Chen, Xiaoqian Shen, Xiang Li, and Mohamed Elhoseiny. Minigpt-4: Enhancing vision-language understanding with advanced large language models, 2023. 1, 2, 5
- [38] Younan Zhu, Linwei Tao, Minjing Dong, and Chang Xu. Mitigating object hallucinations in large vision-language models via attention calibration, 2025. 2, 3
- [39] Kaiwen Zuo and Yirui Jiang. Medhallbench: A new benchmark for assessing hallucination in medical large language models, 2025. 1

# Attention-space Contrastive Guidance for Efficient Hallucination Mitigation in LVLMs

## Supplementary Material

### A. Implementation Details

#### A.1. Models.

We evaluate ACG on three open-source large vision-language models (LVLMs) with diverse language backbones and vision-language connectors: LLaVA-1.5, MiniGPT-4, and Qwen-VL-Chat.

**LLaVA-1.5.** [19] LLaVA-1.5 adopts a CLIP ViT-L/336px vision encoder and a Vicuna language model built on the LLaMA architecture, connected by a fully connected MLP-based vision-language projector. The CLIP encoder produces 576 visual tokens per image, which are mapped into the language model token embedding space by a two-layer MLP and then concatenated with text tokens. The model is trained in a two-stage pipeline: vision-language alignment on image-text pairs, followed by visual instruction tuning on conversational multimodal data.

**MiniGPT-4.** [37] MiniGPT-4 uses the visual frontend of BLIP-2: a ViT-G/14 visual encoder from EVA-CLIP followed by a Q-Former that compresses dense image features into a small set of visual tokens. The Q-Former employs a fixed set of learnable queries (32 in our setup), so each image is represented as 32 visual tokens. These Q-Former outputs are passed through a single linear projection layer to align them with the Vicuna language model embedding space, and the projected visual tokens are then fed into Vicuna as a soft prompt for generation.

**Qwen-VL-Chat.** [2] Qwen-VL-Chat builds on the Qwen language model and a ViT-bigG visual encoder from Open-CLIP. Image features are first extracted by the ViT encoder and then compressed by a position-aware vision-language adapter: a single-layer cross-attention module with learnable query embeddings. We use the default configuration with 256 queries, yielding 256 visual tokens per image, which are fed into the language model as a fixed-length visual token block.

#### A.2. Benchmarks.

**POPE.** [17] POPE (Precision-based Object Probing Evaluation) evaluates object hallucination through binary object-presence queries. For each image, the model answers questions of the form “Is there a `<object>` in the image?” with a balanced mixture of present and absent objects. POPE provides three complementary

evaluation sets: (1) *Random*: object categories are sampled uniformly from the vocabulary, reflecting unbiased hallucination performance; (2) *Popular*: focuses on frequently occurring objects in large-scale training corpora, testing whether the model over-relies on language priors; (3) *Adversarial*: selects semantically or visually confusable objects (e.g., querying “cat” for dog images), stressing context-induced hallucination.

**Metrics.** POPE reports Accuracy, Precision, Recall, and F1.

**CHAIR.** [24] CHAIR (Caption Hallucination Assessment with Image Re-annotation) measures hallucination in image captioning by aligning object mentions in generated captions with COCO ground-truth annotations. Any object mentioned in the caption but absent in the image is regarded as hallucinated.

**Metrics.** CHAIR provides two metrics:

$$\text{CHAIR}_i = \frac{\#\text{hallucinated object instances}}{\#\text{all mentioned objects}},$$
$$\text{CHAIR}_s = \frac{\#\text{captions containing hallucination}}{\#\text{total captions}}.$$

$\text{CHAIR}_i$  captures object-level hallucination frequency, while  $\text{CHAIR}_s$  measures how often a caption contains any hallucination.

**Why F1 is Reported Alongside  $\text{CHAIR}_s$  and  $\text{CHAIR}_i$ .**  $\text{CHAIR}_i$  and  $\text{CHAIR}_s$  measure hallucination from the perspective of “how often” hallucinated objects appear in a caption, but they do not consider whether the model successfully mentions objects that actually exist in the image. In contrast, the object-level F1 score captures the balance between avoiding hallucinated objects (precision) and correctly mentioning ground-truth objects (recall). A model may achieve a low CHAIR score simply by producing overly conservative captions that omit many valid objects, which results in low recall. Therefore, reporting F1 alongside  $\text{CHAIR}_i$  and  $\text{CHAIR}_s$  provides a more complete view of caption quality, distinguishing models that truly reduce hallucination from those that merely under-describe the image.

**MMHal-Bench.** [28] MMHal-Bench is a hallucination-centric benchmark specifically designed to diagnose the visual grounding reliability of large vision-language models (LVLMs). The dataset contains images paired with care-

fully constructed natural-language queries that target reasoning types known to induce hallucination, such as object attributes, spatial relations, counting, and adversarially misleading premises. Unlike captioning-based or binary object-probing benchmarks, MMHal-Bench evaluates open-ended, reasoning-intensive responses, where hallucinations arise not only in object mentions but also in relational, numerical, or contextual inferences. Each query expects a concise, grounded answer that can be automatically judged for hallucination and informativeness using an LLM-as-a-judge protocol.

The benchmark evaluates hallucination across several reasoning dimensions that are known to induce failure in LVLMs:

- **ATTR (Object Attributes):** questions about appearance attributes such as color, shape, texture, or material (e.g., “What color is the man’s jacket?”).
- **ADV (Adversarial Objects):** queries intentionally designed to include objects not present in the image (e.g., “What is the dog holding in its hand?”). This category tests the model’s robustness to adversarial wording and its ability to reject false premises.
- **COMP (Comparisons):** relational comparisons of size, number, or attributes between two or more objects (e.g., “Which cup is larger?”).
- **COUNT (Counting):** numerical reasoning about the number of instances.
- **SPAT (Spatial Relations):** reasoning about object positions or geometric relations (e.g., “Where is the bicycle relative to the car?”).
- **ENV (Environmental / Scene Inference):** global contextual reasoning about the environment, scene type, or high-level situational cues (e.g., “Is this an indoor or outdoor scene?”).

**Evaluation Protocol.** MMHal adopts an LLM-as-a-judge evaluation pipeline in which GPT-4 scores each model response along two dimensions: *informativeness* and *hallucination*. For every image–query pair, GPT-4 is prompted to evaluate (1) how informative the response is on a 0–6 scale, where 0 indicates an unhelpful or irrelevant answer and 6 indicates a fully grounded, complete, and contextually appropriate answer; and (2) whether the response contains any hallucinated visual content (binary judgment: hallucinated / not hallucinated). This protocol enables the benchmark to assess both the usefulness and the visual faithfulness of a model’s answer.

### A.3. Baseline Methods and Hyperparameters

For baseline comparisons, we evaluated VCD [14], PAI [21], and VISTA [18]. All baselines were reproduced using their official code repositories, and all experiments were conducted under a unified greedy decoding setting. For hyperparameters, we followed the configurations re-

Table 6. Effect of guidance scale  $\gamma$  on CHAIR (max 128) for LLaVA-1.5. We report sentence-level hallucination ( $\text{CHAIR}_s$ ), instance-level hallucination ( $\text{CHAIR}_i$ ), F1, and average caption length (Len). We choose  $\gamma = 2.4$  as our operating point.

$\gamma$	$\text{CHAIR}_s (\downarrow)$	$\text{CHAIR}_i (\downarrow)$	F1 ( $\uparrow$ )	Len
1.0	47.4	12.8	77.8	91.6
1.3	48.6	12.9	78.1	89.4
1.5	44.8	11.6	78.1	88.2
1.7	42.4	10.3	79.1	84.9
1.9	36.4	8.6	79.3	83.5
2.0	33.0	8.0	79.0	82.1
2.1	34.2	7.6	77.6	80.8
2.2	27.6	6.4	76.7	77.5
2.3	27.8	6.6	75.5	74.9
<b>2.4</b>	<b>21.0</b>	<b>4.8</b>	<b>74.4</b>	72.4
2.5	19.2	4.8	72.4	67.2
2.6	15.4	4.8	68.0	58.7
2.7	12.8	4.9	64.7	51.0
2.8	9.0	4.8	60.4	42.0
2.9	7.2	6.0	56.1	33.9
3.0	6.2	4.2	51.8	25.8

Table 7. Effect of guidance scale  $\gamma$  on CHAIR (max 128) for MiniGPT-4. We again report  $\text{CHAIR}_s$ ,  $\text{CHAIR}_i$ , F1, and average caption length (Len). We choose  $\gamma = 0.3$  as our operating point.

$\gamma$	$\text{CHAIR}_s (\downarrow)$	$\text{CHAIR}_i (\downarrow)$	F1 ( $\uparrow$ )	Len
0.10	27.6	9.0	70.6	72.9
0.15	24.4	7.9	71.0	69.4
0.20	21.0	6.8	70.3	63.5
0.25	16.6	5.2	69.5	59.1
<b>0.30</b>	<b>10.8</b>	<b>3.3</b>	<b>68.0</b>	66.3
0.35	6.2	2.5	63.2	73.6
0.40	2.6	1.6	54.3	94.9

ported in the original papers unless otherwise noted. An exception is VISTA: as prior reports indicate that the official hyperparameters do not reproduce the reported results, we conducted a parameter search and set `vsv-lambda` to 0.01 for POPE and 0.15 for CHAIR.

## B. Behavior Across Guidance Scale and Depth

### B.1. Guidance Scale Selection.

For each LVLM, we select the guidance scale  $\gamma$  on the CHAIR (max 128 tokens) benchmark by sweeping  $\gamma$  and monitoring the trade-off between hallucination and caption quality. Concretely, we measure sentence-level hallucination ( $\text{CHAIR}_s$ ), instance-level hallucination ( $\text{CHAIR}_i$ ), F1, and the average caption length (Len) under greedy decod-

Table 8. Layer-block ablation on LLaVA-1.5 (CHAIR, max 128). We apply ACG only to a given layer block and report CHAIR<sub>s</sub>, CHAIR<sub>i</sub>, F1, and average caption length (Len).

(a) Early (layers 1–8, ACG-Fast)					(b) Early–mid (layers 9–16)				
$\gamma$	CHAIR <sub>s</sub>	CHAIR <sub>i</sub>	F1	Len	$\gamma$	CHAIR <sub>s</sub>	CHAIR <sub>i</sub>	F1	Len
0.5	47.8	12.6	77.1	93.4	0.5	49.2	14.0	76.6	94.3
1.0	46.0	13.1	77.0	91.9	1.0	49.0	14.2	76.4	93.7
1.5	43.2	12.2	77.6	88.3	2.0	53.6	14.4	75.9	92.4
2.0	35.8	10.2	77.4	82.2	2.5	51.0	13.9	76.3	92.0
2.5	28.0	7.1	77.5	77.6	3.0	53.6	15.3	74.8	90.7
3.0	19.0	5.3	69.8	68.0	6.0	38.0	11.1	74.8	79.2
6.0	0.2	2.9	13.2	15.6	8.0	14.2	5.7	56.6	45.9
10.0	0.0	0.0	0.2	1.2	10.0	2.2	2.1	22.5	16.3

(c) Mid–late (layers 17–24)					(d) Late (layers 25–32)				
$\gamma$	CHAIR <sub>s</sub>	CHAIR <sub>i</sub>	F1	Len	$\gamma$	CHAIR <sub>s</sub>	CHAIR <sub>i</sub>	F1	Len
0.5	46.4	12.6	77.6	94.4	0.5	44.0	12.8	76.9	93.5
1.0	46.4	12.5	78.3	93.4	1.0	43.8	12.2	77.4	93.7
1.5	43.8	12.5	78.2	94.6	1.5	44.2	12.1	77.7	93.1
2.5	47.2	12.7	78.1	95.6	2.0	41.8	11.4	78.4	93.6
4.0	51.8	12.7	76.6	95.9	2.5	40.4	10.7	78.6	93.0
6.0	42.6	10.7	77.4	95.6	4.0	39.4	10.2	78.9	92.5
8.0	40.2	9.2	76.3	95.0	6.0	37.8	9.7	78.2	93.4
10.0	35.8	7.0	73.4	91.8	10.0	36.0	8.8	75.7	90.7

ing, and choose an operating point that (i) substantially reduces CHAIR<sub>i</sub> compared to the greedy baseline, while (ii) keeping F1 within roughly 5% of the baseline and (iii) avoiding degenerate overly short captions. The selected  $\gamma$  is then reused for all CHAIR (both max tokens 64 and 128) and POPE experiments on the corresponding model.

This protocol is consistent with prior training-free hallucination mitigation methods. For instance, PAI [21] tunes its scaling parameters by sweeping on the CHAIR benchmark itself, jointly considering CHAIR and F1, without introducing a separate validation split.

Table 6 shows the sweep for LLaVA-1.5. As  $\gamma$  increases from 1.0 to 2.4, CHAIR<sub>i</sub> consistently decreases from 12.8 to 4.8, while F1 only drops from 77.8 to 74.4 and the average length remains moderate (72.4 tokens). Beyond  $\gamma = 2.4$ , CHAIR<sub>i</sub> continues to decrease but F1 and length collapse sharply (e.g., F1 = 51.8 and Len = 25.8 at  $\gamma = 3.0$ ), indicating an over-aggressive regime. We therefore choose  $\gamma = 2.4$  as the canonical operating point for LLaVA-1.5. A similar trend is observed for MiniGPT-4 in Table 7. We select  $\gamma = 0.3$ , while avoiding the more unstable behavior at larger  $\gamma$ .

## B.2. Layer-block configurations.

We also study where to apply ACG inside the LLaVA-1.5 decoder by restricting the guidance to different layer blocks. Table 8 reports CHAIR<sub>s</sub>, CHAIR<sub>i</sub>, F1, and average caption length (Len) on CHAIR (max 128) when we apply ACG only to early (layers 1–8), early–mid (9–16), mid–late (17–24), or late (25–32) blocks. We denote the early-only variant (layers 1–8) as *ACG-Fast*, which offers a good trade-off between hallucination reduction and efficiency.

**Why early layers help: approximation bias and contextual leakage.** The block-wise trend is both architectural and methodological. Architecturally, early transformer layers perform the first rounds of text–vision routing and token alignment; small attention shifts there propagate through the stack, yielding large reductions in hallucination for relatively modest  $\gamma$ . Methodologically, our masked-unconditional surrogate  $O_{\text{uncond}}^{\text{mask}}$  deviates from the true text-only path due to contextual leakage and softmax redistribution. This approximation bias compounds with depth as more context is mixed into the representations, so the guidance direction becomes increasingly contaminated by text-induced bias in deeper blocks. Shallow layers therefore provide a cleaner guidance signal, while deeper layers

Table 9. Category-wise informativeness and hallucination rate on MMHal.

$\gamma$	Avg	ATTR	ADV	COMP	COUNT	SPAT	ENV	HOL	OTH	Hallucination Rate
0 (Vanilla)	1.94	2.25	1.42	2.67	1.50	1.92	2.92	1.75	1.08	0.59
1	2.06	2.25	1.33	2.17	1.33	2.75	3.25	2.08	1.33	0.56
1.5	2.07	2.50	1.08	1.75	1.92	2.00	3.25	2.08	2.00	0.57
2	2.12	2.50	1.67	1.92	1.58	2.25	3.25	2.00	1.83	0.53
2.4	2.01	2.58	2.00	1.83	1.17	2.25	3.25	1.17	1.83	0.56

require larger guidance coefficients to achieve comparable hallucination reduction.

Empirically, this matches the trends in Table 8. **Early (1–8)** reaches  $\text{CHAIR}_i = 7.1$  at  $\gamma = 2.5$  ( $\text{F1} = 77.5$ ,  $\text{Len} = 77.6$ ) and  $\text{CHAIR}_i = 5.3$  at  $\gamma = 3.0$  ( $\text{Len} = 68.0$ ), whereas **Mid-late (17–24)** needs  $\gamma = 10.0$  to approach  $\text{CHAIR}_i = 7.0$  ( $\text{F1} = 73.4$ ,  $\text{Len} = 91.8$ ). **All (1–32)** attains the strongest reduction overall in the main paper ( $\text{CHAIR}_i = 4.8$  at  $\gamma = 2.4$ ). These patterns support our interpretation that cross-modal bias is best corrected where text and vision first interact, and that the masked-unconditional approximation is most faithful in the early layers, making guidance most effective there.

## C. Quantitative & Qualitative Results

### C.1. Detailed MMHal-Bench Scores.

In addition to the MMHal-Bench scores reported in main paper, we also provide results across multiple values of  $\gamma$ , ranging from 1.0 to 2.4. As shown in Table 9, our method consistently achieves higher scores and lower hallucination rates than the vanilla model, achieving highest score at  $\gamma = 2$ .

### C.2. Additional examples on MMHal-Bench.

Figure 6 provides additional examples from MMHal-Bench. For the environmental reasoning query, vanilla LLaVA-1.5 describes the scene as **sunny** and well-lit, following language priors, whereas our method correctly answers that the weather appears **dark** because the cabin is dimly lit by indoor lights. For the counting-style question, vanilla misreads the fastest runner’s bib number as **1019**, but our method outputs the correct number **1097**, aligned with the ground-truth. These examples support our quantitative findings that ACG improves informativeness while reducing hallucination on MMHal-Bench.

### C.3. CHAIR examples on open-ended generation.

Figure 7 shows CHAIR-style captioning examples. In the toaster image (top), vanilla LLaVA-1.5 and the PAI baseline hallucinate background objects such as a **sink**, **cup**, or even misclassify the appliance as a **toaster oven**, while our method only mentions the grounded **toaster** and its visible

attributes. In the second example (bottom), both baselines repeatedly refer to a **table** and a **knife** that are not clearly present in the image. ACG instead concentrates on the truly visible entities—**glasses**, **paper**, and **scissors**—showing that attention-space guidance effectively suppresses spurious background objects while preserving the core scene semantics.

## D. Limitation and Future Work

Here we discuss two key limitations of our method and potential directions for future work.

**Architecture-specific behavior.** ACG assumes a standard LVLM design where visual tokens appear as a contiguous block in the decoder input. However, architectures such as InstructBLIP employ Q-Former-based encoders or cross-attention modules that interleave or embed visual features directly into the text stream. In such settings, simply masking visual-key positions does not fully remove visual information, since contextualized text embeddings may already encode fused vision features. Future work may develop architecture-aware masking strategies or alternative ways of constructing text-only paths that better match each model’s multimodal fusion mechanism.

**Depth-dependent sensitivity.** ACG exhibits noticeable depth-dependent behavior: early layers respond strongly to guidance, while mid-to-late layers require significantly larger  $\gamma$  to achieve comparable hallucination reduction. This suggests that visual grounding signals decay across depth, and that a uniform guidance scale may under-correct or over-correct depending on the layer. A more adaptive design—such as depth-specific scaling, head-wise weighting, or learned guidance schedules—could stabilize ACG across layers and further improve hallucination mitigation.

Visual Input :



Query :

What was the weather like when this photo was taken?

[Ground Truth Answer]

When this photo was taken, it was already night and the sky was dark.

[LLaVA-1.5]

The weather in the photo appears to be **sunny**, as the room is well-lit and the **sunlight** is shining through the windows.

[Ours]

The weather in the photo was **dark**, as the room is dimly lit, and the cabin is lit up by a light.

Visual Input :



Query :

What number is the fastest girl wearing in the picture?"

[Ground Truth Answer]

The fastest girl in the picture is wearing number 1097.

[LLaVA-1.5]

The fastest girl in the picture is wearing the number **1019**.

[Ours]

**1097**

Figure 6. Success examples on MMHal-Bench. In the first example, vanilla LLaVA-1.5 hallucinates a bright and **sunny** environment, whereas our method correctly infers that the cabin is **dark** and lit by artificial light. In the second example, vanilla misreads the runner's bib number as **1019**, while our method outputs the correct number **1097**, matching the ground-truth answer.

Visual Input :



Query :

Please help me describe the image in detail.

[LLaVA-1.5]

The image features a silver toaster sitting on a tiled countertop. (...) In the background, there is a sink visible, suggesting that the kitchen is well-equipped for cooking and cleaning tasks. Additionally, there is a cup placed on the countertop, possibly for holding a beverage or other items.

[PAI]

The image features a silver toaster oven sitting on a tiled countertop. The toaster oven is placed on a tile countertop, and it appears to be a Cuisin brand toaster oven. The toaster oven is turned on, and it is placed on a tile countertop.

[Ours]

The image features a toaster on a green tiled countertop. The toaster is a Charger toaster, and it is sitting on a tile counter. The toaster is silver and has a black cord plugged into it.

Visual Input :



Query :

Please help me describe the image in detail.

[LLaVA-1.5]

The image features a man wearing glasses, sitting at a table and cutting a piece of paper with a pair of scissors. (...) The man is using a knife to cut the paper, which is placed on the table in front of him.

[PAI]

The image features a man wearing glasses, who is cutting a piece of paper with a pair of scissors. He is focused on the task at hand, and the paper is placed on a table. (...) The man is focused on his task, and the paper is placed on a table, which is located in the foreground of the image.

[Ours]

The man is wearing glasses and cutting a piece of paper with a pair of scissors. He is holding the paper with his fingers and is looking down at it. The man is wearing a white shirt and glasses.

Figure 7. Qualitative CHAIR examples comparing vanilla LLaVA-1.5, PAI, and our ACG method. For each caption, we highlight object tokens: blue tokens denote objects that are grounded in the image, while red tokens indicate hallucinated objects (e.g., sink, cup, table, knife). Compared to the baselines, ACG removes spurious background objects and focuses on the truly visible entities (e.g., the toaster, glasses, paper, and scissors).